Progress In Electromagnetics Research, PIER 54, 137–154, 2005

EFFECTIVE EXPLOITATION OF MULTI-VIEW DATA THROUGH THE ITERATIVE MULTI-SCALING METHOD — AN EXPERIMENTAL ASSESSMENT

M. Donelli, D. Franceschini, G. Franceschini, and A. Massa

Department of Information and Communication Technologies
University of Trento
Via Sommarive, 14-38050 Trento, Italy

Abstract—The reconstruction capabilities of a microwave imaging algorithm can be enhanced by exploiting a multi-view measurement set-up. In the past, different researches have proved that collecting scattering data by probing the unknown scenario from different incidence angles, it allows to acquire more information on the scenario under test. This paper is aimed at verifying such an assumption in a real scenario when the Iterative Multi-Scaling Approach (IMSA) is used to fully exploit multi-view data. In fact, unlike synthetic data, in a real environment more measurements introduce larger systematic errors that could affect the physical constraints used in the inversion procedure and, consequently, the reconstruction process. Thus, the analysis is carried out by considering a set of experimental data concerning different scattering configurations involving single and multiple dielectric scatterers.

1. INTRODUCTION

Each microwave imaging system, aimed at detecting, locating and imaging unknown objects located in inaccessible areas (for a general overview and some applications, see [1–4] and the references cited therein), is constituted by two main parts. The algorithmic part consists of a processing unit that performs the inversion of the scattered field data by means of a suitable numerical procedure. On the other hand, the electro-mechanical set-up allows the collection of the measures of the electromagnetic field scattered by the scenario under test. Usually, the measurement setup is designed according to the experimental arrangement, which strongly depends on the problem geometry.

Let us consider an ideal situation where there are not limits to the collection of scattered field measures. Even in such a favorable situation, the amount of collectable information from the measurements is limited [5]. In order to enlarge the information content arising from scattered data, multi-view systems [6] (i.e., systems consisting of a rotating setup that probes the investigation area from different angles of illumination) are commonly used. The imaging process benefits by this improvement as theoretically shown in [7] and numerically confirmed in [8] with several synthetic experiments.

But, the same can be said for real experiments? And, it is true whatever the inversion procedure? And, what is the amount of the improvement over single-view systems? The generalization from synthetic to experimental environments is not obvious. In many practical situations, several unavoidable errors and inaccuracies occur. Just to do some examples, the environmental noise corrupts the measures. Such an event adds to the interferences due to the coupling among emitters and receivers and to the positioning errors of the mechanical system. Consequently, a microwave imaging algorithm operates on an unreliable dataset that could introduce false physical constraints and bring the retrieval process towards false solutions.

On the other hand, the increasing of the number of scattering data corresponds to an enlargement of the solution space and of its dimensionality. Therefore, effective and reliable inversion techniques, able to deal with such a situation, should be used. In such a framework, this paper focuses on the reconstruction capabilities of the IMSA [9, 10] when dealing with real data to assess "if" and "how much" this method is able to fully exploit multi-view data.

The paper is organized as follows. The mathematical formulation of the IMSA will be resumed in Section 2 to introduce in Section 3 a representative numerical analysis concerning real data scattered by

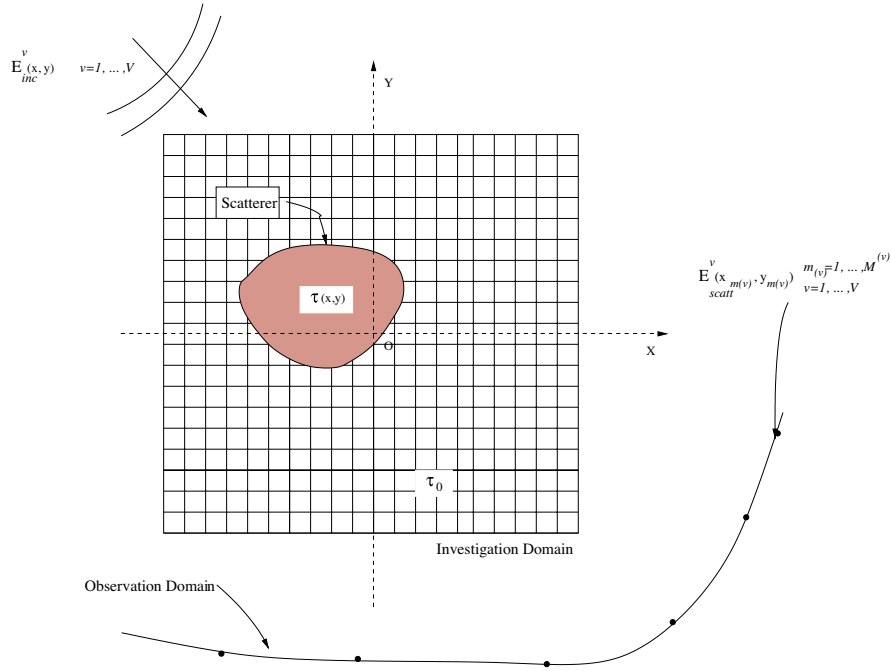

Figure 1. Problem geometry.

single- and multiple-scatterers configurations. Some conclusions and remarks will be drawn in Section 4.

2. MATHEMATICAL FORMULATION

Let us consider the two-dimensional scenario depicted in Figure 1. An unknown scatterer, located in an investigation domain D_I, interacts with a set of known probing electromagnetic fields, $E^v_{inc}(x, y)$, $v = 1, ..., V$. The background is assumed lossless and non-magnetic while the object is described by means of the contrast function $\tau(x, y) = \varepsilon_r(x, y) - 1 - j\frac{\sigma(x,y)}{2\pi f \varepsilon_0}$, $(x, y) \in D_I$, $\varepsilon_r(x, y)$ and $\sigma(x, y)$ being the dielectric permittivity and the electric conductivity, respectively. The electromagnetic scattered field $E^v_{scatt}\left(x_{m_{(v)}}, y_{m_{(v)}}\right) \triangleq E^v_{tot}\left(x_{m_{(v)}}, y_{m_{(v)}}\right) - E^v_{inc}\left(x_{m_{(v)}}, y_{m_{(v)}}\right)$ ($E^v_{tot}(x, y)$ being the electric field in the presence of the scatterer) is collected in $m_{(v)} = 1, ..., M_{(v)}$ positions belonging to an observation domain D_M external to D_I.

From a mathematical point of view, the interactions among the

scatterer and incident electromagnetic fields are described through the Lippmann-Schwinger integral equations [11], discretized according to the Richmond's procedure [12]:

$$\begin{aligned} & E^v_{scatt}\left(x_{m_{(v)}},\, y_{m_{(v)}}\right) \\ = \;& \Im^{v,m}_{Data}\left\{\tau\left(x_n, y_n\right),\, E^v_{tot}\left(x_n,\, y_n\right); n = 1, \cdots, N; v = 1, \cdots, V\right\} \\ & \left(x_{m_{(v)}},\, y_{m_{(v)}}\right) \in D_M \qquad m_{(v)} = 1, \cdots, M_{(v)}; \quad v = 1, \cdots, V \end{aligned} \tag{1}$$

$$\begin{aligned} & E^v_{inc}\left(x_n,\, y_n\right) \\ = \;& \Im^{v,n}_{State}\left\{\tau\left(x_n,\, y_n\right),\, E^v_{tot}\left(x_n,\, y_n\right);\, n = 1, \cdots, N;\, v = 1, \cdots, V\right\} \\ & \left(x_n,\, y_n\right) \in D_I \qquad n = 1, \cdots, N; \quad v = 1, \cdots, V \end{aligned} \tag{2}$$

where $\tau(x,\, y) = \sum_{n=1}^{N} \tau\left(x_n,\, y_n\right) F_n\left(x,\, y\right)$ and $E^v_{tot}(x,\, y) = \sum_{n=1}^{N} E^v_{tot}\left(x_n,\, y_n\right) F_n\left(x,\, y\right)$, $F_n\left(x,\, y\right)$ being the nth basis function; $\Im_{ext}$ and $\Im_{int}$ are the external and internal scattering operators [11].

Such a formulation provides a set of non-linear equations characterized by an intrinsic ill-conditioning. Then, the arising algebraic system (1)–(2) is commonly solved by recasting the problem to the minimization of a suitable cost function.

However, to better exploit the information content of scattered data, a multi-scaling strategy [10] is used by defining a multi-resolution expansion of the unknown quantities as follows

$$\begin{aligned} & \tau(x,\, y) = \sum_{r=1}^{R} \sum_{n_{(r)}=1}^{N_{(r)}} \tau\left(x_{n_{(r)}}, y_{n_{(r)}}\right) F_{n_{(r)}}\left(x,\, y\right) \\ & \left(x_{n_{(r)}}, y_{n_{(r)}}\right) \in D_I \qquad n_{(r)} = 1, ..., N_{(r)}; \quad r = 1, ..., R = (s+1) \end{aligned} \tag{3}$$

$$E^v_{tot}\left(x,\, y\right) = \sum_{r=1}^{R} \sum_{n_{(r)}=1}^{N_{(r)}} E^v_{tot}\left(x_{n_{(r)}},\, y_{n_{(r)}}\right) F_{n_{(r)}}\left(x,\, y\right) \tag{4}$$

where R defines the maximum order of the resolution (being r the resolution index), and by iteratively performing (at each step s of the process) a reconstruction with an increment of the spatial resolution in the Region-of-Interest (RoI) to which the scatterer belongs.

For a detailed description, let us consider the flow-chart shown in Fig. 2. At the "*initialization*" ($s = 0$), the investigation domain is uniformly partitioned in $N_{(R)}$ ($R = 1$) square sub-domains and the problem unknowns are set to the background configuration $\left(E^{v\,(s)}_{tot}\left(x_{n_{(R)}},\, y_{n_{(R)}}\right)\right|_{s=0} = E^v_{inc}\left(x_{n_{(R)}},\, y_{n_{(R)}}\right)$ and

$\tau^{(s)}\left(x_{n_{(R)}}, y_{n_{(R)}}\right)\Big|_{s=0} = \tau_0,\ n_{(R)} = 1, ..., N_{(R)})$. Moreover, the multi-resolution cost function is defined [13]

$$\begin{aligned}
&\Phi\Bigg\{\tau_{(q)}^{(s)}\left(x_{n_{(r)}}, y_{n_{(r)}}\right),\ E_{tot}^{v\,(s)}\left(x_{n_{(r)}}, y_{n_{(r)}}\right);\\
&\qquad\qquad \begin{array}{cc} q = 1, .., Q_{(s)}; & r = 1, ..., R = s; \\ n_{(r)} = 1, ..., N_{(r)}; & v = 1, ..., V \end{array}\Bigg\}\\
= &\Bigg\{\sum_{q=1}^{Q_{(s)}}\sum_{v=1}^{V}\sum_{m_{(v)}=1}^{M_{(v)}}\left|E_{scatt}^{v}\left(x_{m_{(v)}}, y_{m_{(v)}}\right)\right.\\
&-\sum_{r=1}^{R}\sum_{n_{(r)}=1}^{N_{(r)}}\left\{w^{(q)}\left(x_{n_{(r)}}, y_{n_{(r)}}\right)\tau_{(q)}^{(s)}\left(x_{n_{(r)}}, y_{n_{(r)}}\right)\right.\\
&\left.\left.E_{tot}^{v\,(s)}\left(x_{n_{(r)}}, y_{n_{(r)}}\right)G_{2d}\left(A_{n_{(r)}}, \rho_{n_{(r)}m_{(v)}}\right)\right\}\right|^2\Bigg\}\\
&+\Bigg\{\sum_{q=1}^{Q_{(s)}}\sum_{v=1}^{V}\sum_{r=1}^{R}\sum_{n_{(r)}=1}^{N_{(r)}}\left\{w^{(q)}\left(x_{n_{(r)}}, y_{n_{(r)}}\right)\left|E_{inc}^{v}\left(x_{n_{(r)}}, y_{n_{(r)}}\right)\right.\right.\\
&-\Bigg[E_{tot}^{v\,(s)}\left(x_{n_{(r)}}, y_{n_{(r)}}\right)+\sum_{u_{(r)}=1}^{N_{(r)}}\left\{\tau_{(q)}^{(s)}\left(x_{u_{(r)}}, y_{u_{(r)}}\right)\right.\\
&\left.\left.\left.E_{tot}^{v\,(s)}\left(x_{u_{(r)}}, y_{u_{(r)}}\right)G_{2d}\left(A_{u_{(r)}}, \rho_{u_{(r)}n_{(r)}}\right)\right\}\Bigg]\right|\Bigg\}^2\Bigg\}
\end{aligned} \tag{5}$$

where

$$w^{(q)}(x_{n_{(r)}}, y_{n_{(r)}}) = \begin{cases} 0 & \text{if } (x_{n_{(r)}}, y_{n_{(r)}}) \notin D_{O(s-1)}^{(q)} \\ 1 & \text{if } (x_{n_{(r)}}, y_{n_{(r)}}) \in D_{O(s-1)}^{(q)} \end{cases}$$

Q being the number of scatterers and $D_O^{(q)}, q = 1, ..., Q$ the corresponding RoIs, where the synthetic zoom will be performed; $Q_{(s=0)} = 1$.

Successively ($s \leftarrow s+1$), the unknowns are updated

$$\tau^{(s)}\left(x_{n_{(R)}}, y_{n_{(R)}}\right)\Big|_{s=1} = \arg\left\{min_{\tau_{(q)}^{(0)}}\left[\Phi^{(0)}\right]\right\} \tag{6}$$

$$E_{tot}^{v\,(s)}\left(x_{n_{(R)}},\ y_{n_{(R)}}\right)\Big|_{s=1} = \arg\left\{min_{E_{tot}^{v\,(s)}}\left[\Phi^{(0)}\right]\right\} \tag{7}$$

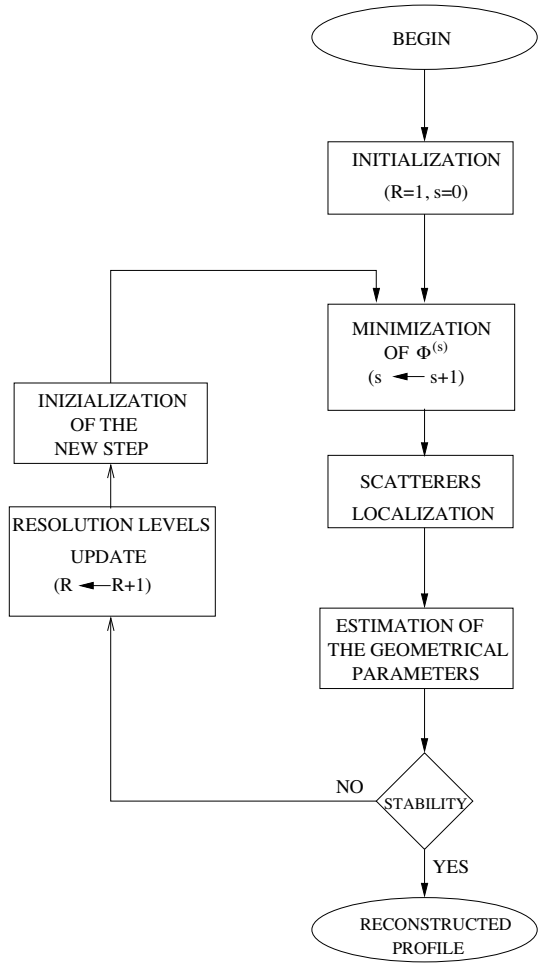

Figure 2. Flow chart of the Iterative Multi-Scaling Method.

where $\Phi^{(0)} = \Phi\left\{\tau_{(q)}^{(0)}\left(x_{n_{(r)}}, y_{n_{(r)}}\right), E_{tot}^{v\,(0)}\left(x_{n_{(r)}}, y_{n_{(r)}}\right)\right\}$, by minimizing (5) with a suitable optimization algorithm [14].

At this point, the multi-resolution capabilities of the IMSA are fully exploited. The information acquired on the scenario under test allows an estimate of the number $Q_{(s)}$ of scatterers lying in D_I as well as of the geometrical parameters for each of the corresponding RoIs ("*scatterer localization*" phase and "*estimation of the geometrical parameters*" phase — Fig. 2) [13]. The resolution level is enhanced $(R \leftarrow R+1)$ in the RoIs and a new representation of the unknowns

is given according to (3) and (4). Then, a new minimization of $\Phi^{(s)}$ is performed by taking into account the so-defined (6)–(7) trial configuration ("*initialization of the new step*" phase — Fig. 2).

Iteratively, such a procedure is repeated until a stationary condition [13] for the reconstruction is reached ($s = S_{opt}$).

3. NUMERICAL ANALYSIS

In this Section, a numerical analysis will be carried out in order to assess the reconstruction capabilities of the IMSA in regard to the multi-view measurement setup by considering real scattered data. Towards this end, some examples of the experimental dataset available at the "Institute Fresnel" — Marseille, France [15] will be processed.

The first test case considers a single dielectric cylinder (15 mm in radius) located at ($x_{c_{ref}} = 0.0$, $y_{c_{ref}} = -30$ mm) and characterized by a homogeneous contrast $\tau(x, y) = 2.0 \pm 0.3$ estimated with a waveguide method [16]. Concerning the investigation domain, a square domain $L_{DI} = 30$ cm in side has been considered and the reconstruction has been performed by fully exploiting the available scattering data ($M_{(v)} = 49$), but using mono-frequency measurements ($f = 4$ GHz).

The effects of the multi-view setup, in terms of reconstruction errors, will be analyzed by considering the following quantities

$$\rho = \frac{1}{Q}\sum_{q=1}^{Q}\left\{\frac{\sqrt{\left[x^{(q)}_{c_{(S_{opt})}} - x^{(q)}_{c_{ref}}\right]^2 + \left[y^{(q)}_{c_{(S_{opt})}} - y^{(q)}_{c_{ref}}\right]^2}}{\lambda}\right\} \quad \text{(Localization Error)} \tag{8}$$

$$\Delta = \frac{1}{Q}\sum_{q=1}^{Q}\left\{\frac{\left|R^{(q)}_{(S_{opt})} - R^{(q)}_{ref}\right|}{R^{(q)}_{ref}}\right\} \quad \text{(Dimensional Error)} \tag{9}$$

where the sub-script "*ref*" indicates actual quantities[†].

As a first experiment, the reconstruction has been carried out with a *bare* CG-based approach. The investigation domain has been uniformly partitioned in $N = 23 \times 23$ square sub-domains. Fig. 3 shows the behavior of the error figures versus the number of views V used by the multi-view acquisition system. As can be observed, the localization error ρ slightly decreases (from $\rho\rfloor_{V=1} = 1.25 \times 10^{-1}$ up to $\rho\rfloor_{V=30} = 7.17 \times 10^{-2}$) in correspondence with an increasing of the illuminations. On the contrary, an increment of Δ occurs (from

[†] Such quantities are equal to the nominal values reported in [15]

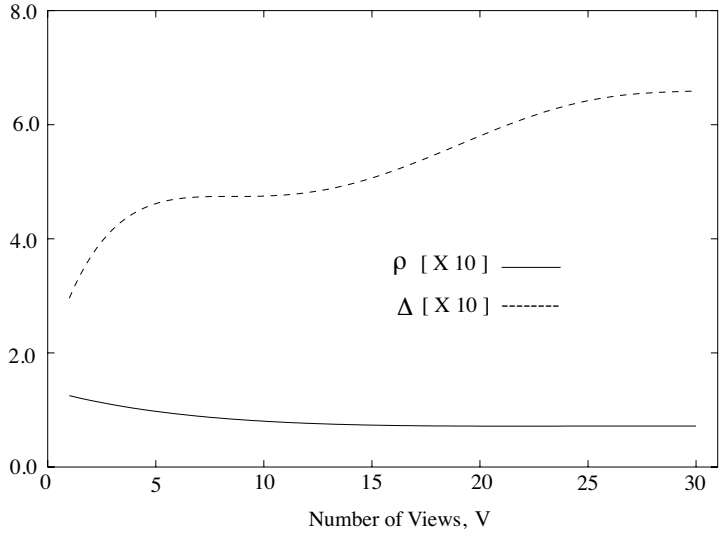

Figure 3. Reconstruction of an off-centered homogeneous circular cylinder (Real dataset "Marseille" [15], "*dielTM_dec8f.exp*") — *CG Approach*. Error figures versus V.

$\Delta\rfloor_{V=1} = 2.96 \times 10^{-1}$ up to $\Delta\rfloor_{V=30} = 6.59 \times 10^{-1}$) as pictorially shown in Fig. 4 where the images of the retrieved profiles when $V = 1$, $V = 6$, $V = 12$, and $V = 24$ are given[‡]. Such a result seems to indicate that the CG-based approach does not fully exploit the advantages of a multi-view system.

Then, in the second experiment, the same problem has been addressed by using the IMSA with the same CG-based optimizer for the cost function minimization (IMSA-CG Approach). According to the amount of information of the scattering data [7] and at the initialization of the multi-scaling process, D_I has been discretized in $N_{(R)} = 10 \times 10$ ($R = 1$) square cells.

For comparison purposes, Fig. 5 shows the behavior of the error figures for the two methods. Concerning the IMSA-CG Approach, the localization accuracy benefits of the enlargement of the available information content (similarly to the CG Approach) as well as the dimensional error, which turns out to be $\Delta < 2.0 \times 10^{-1}$ whatever V. For completeness, Figs. 6(a)–6(b) display the retrieved profiles when $V = 1$, $V = 6$, $V = 12$, and $V = 24$, respectively.

[‡] Please note that the black pixel in the lower right border is used for reference and the dashed line indicates the region occupied by the actual scatterer.

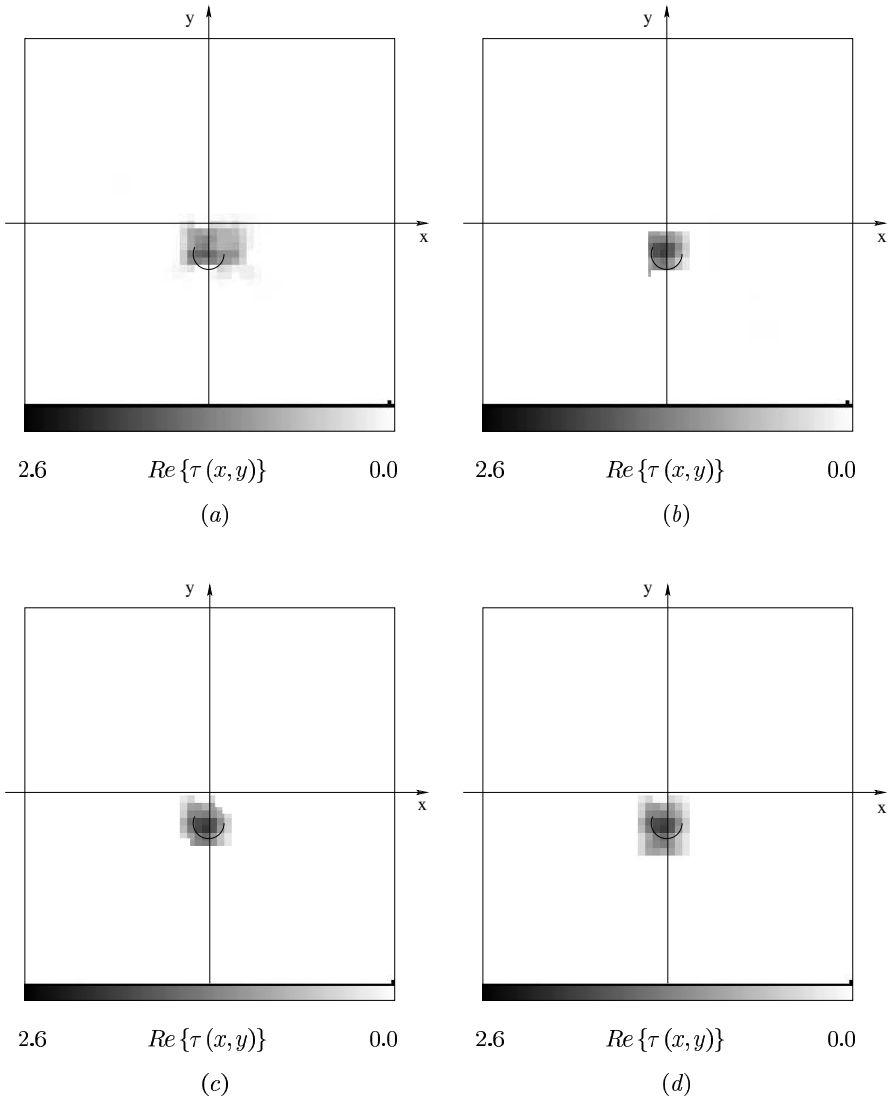

Figure 4. Reconstruction of an off-centered homogeneous circular cylinder (Real dataset"Marseille" [15], "*dielTM_dec8f.exp*") — *CG Approach*. Retrieved profiles at the convergence by considering (a) $V = 1$, (b) $V = 6$, (c) $V = 12$, and (d) $V = 24$ views.

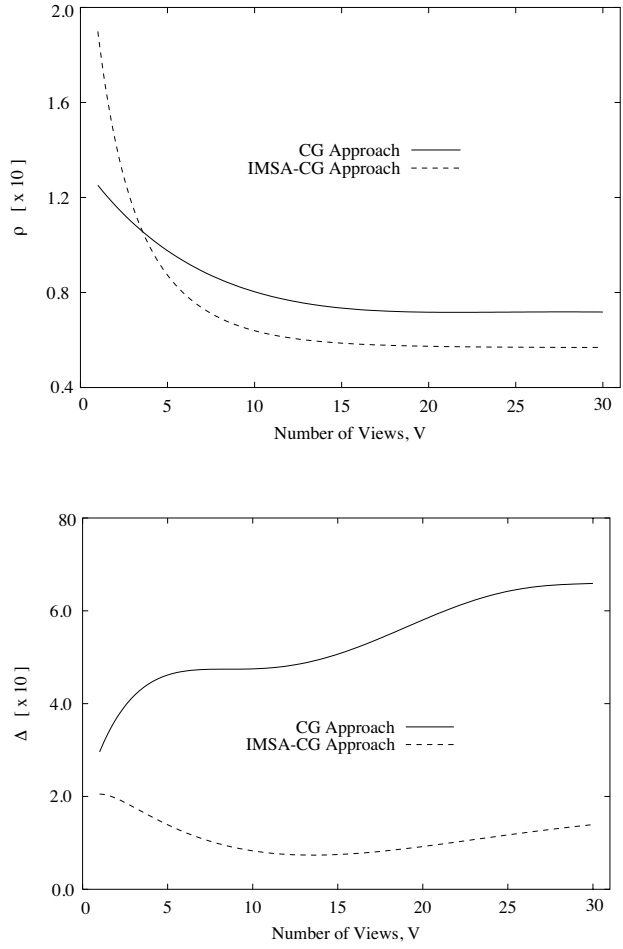

Figure 5. Reconstruction of an off-centered homogeneous circular cylinder (Real dataset "Marseille" [15], "*dielTM_dec8f.exp*") — Error figures versus V for the *CG Approach* and the *IMSA-CG Approach*.

To generalize these indications, the same analysis has been performed for a multiple-scatterers scenario. Towards this aim, the dataset "*twodielTM_8f.exp*" [15], concerned with two circular dielectric ($\tau^{(1)} = \tau^{(2)} = 2.0 \pm 0.3$) cylinders of radius $R_{ref}^{(1)} = R_{ref}^{(2)} = 15\,\text{mm}$ placed 90 mm from each other and located at the nominal coordinates ($x_{c_{ref}}^{(1)} = 0.0$, $y_{c_{ref}}^{(1)} = 45\,\text{mm}$) and ($x_{c_{ref}}^{(2)} = 0.0$, $y_{c_{ref}}^{(2)} = -45\,\text{mm}$), has been processed.

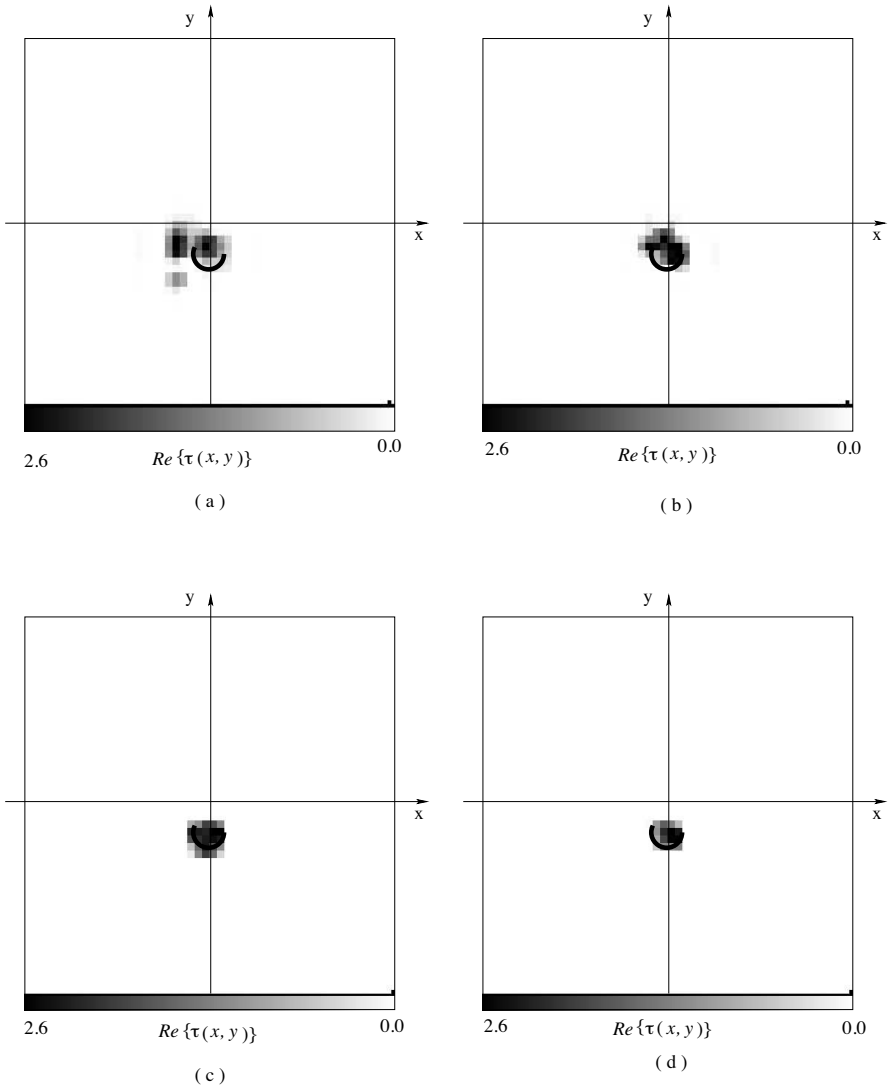

Figure 6. Reconstruction of an off-centered homogeneous circular cylinder (Real dataset "Marseille" [15], "*dielTM_dec8f.exp*") — *IMSA-CG Approach*. Retrieved profiles at the convergence step $s = S_{opt}$ by considering (a) $V = 1$, (b) $V = 6$, (c) $V = 12$, and (d) $V = 24$ views.

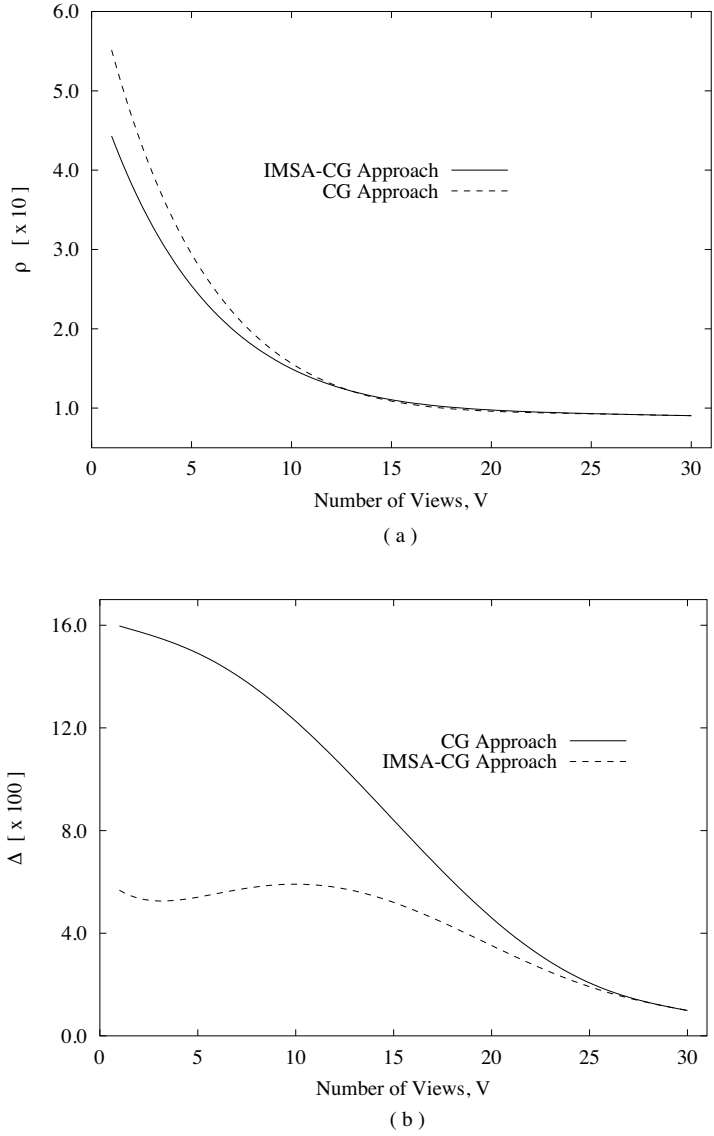

Figure 7. Reconstruction of two homogeneous circular cylinders (Real dataset "Marseille" [15], "*twodielTM_8f.exp*") — Error figures versus V for the *CG Approach* and the *IMSA-CG Approach*.

The achieved results, in terms of localization [Fig. 7(a)] as well as shaping accuracy [Fig. 7(b)], clearly point out an improvement in the reconstruction allowed by the multi-view setup. Whatever the inversion method, ρ and Δ significantly reduces by assessing an advantage in the inversion when more views are used. More in detail, as far as the localization accuracy is concerned, ρ varies between $\rho\rfloor_{V=1} \simeq 6.0 \times 10^{-1}$ and $\rho\rfloor_{V=30} \simeq 1.0 \times 10^{-1}$ and the IMSA-CG

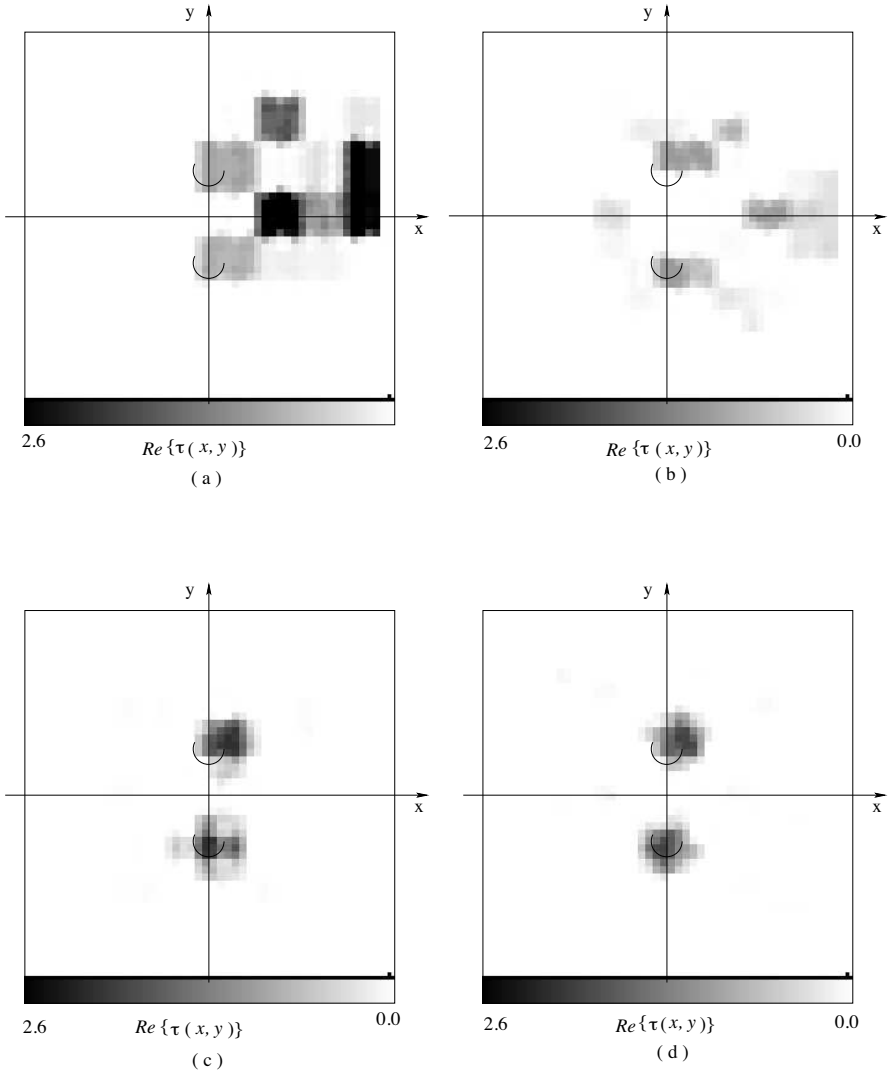

(I)

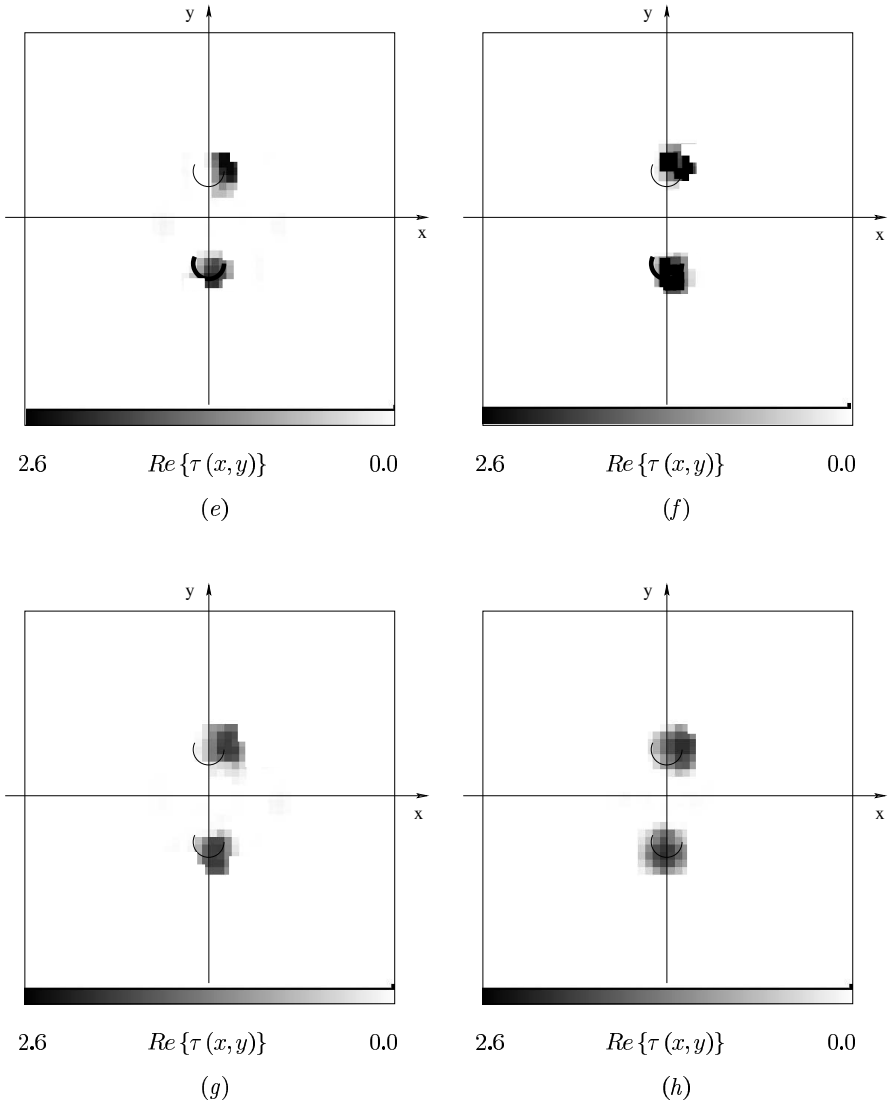

Figure 8. Reconstruction of two homogeneous circular cylinders (Real dataset "Marseille" [15], "*twodielTM_8f.exp*") — Retrieved profiles at the convergence with the (a)*CG Approach*, $V = 1$, (b) *IMSA-CG Approach*, $V = 1$, (c) *CG Approach*, $V = 6$, (d) *IMSA-CG Approach*, $V = 6$, (e) *CG Approach*, $V = 12$, (f) *IMSA-CG Approach*, $V = 12$, (g) *CG Approach*, $V = 24$, and (h) *IMSA-CG Approach*, $V = 24$.

Approach outperforms the bare CG procedure. Similar considerations can be drawn also by observing the behavior of Δ. A non-negligible (if compared to the error values of the CG-based method) improvement in the reconstruction is allowed by the multi-scaling approach when $V \in [1, 16]$ ($\frac{\Delta^{(CG)}\big\rfloor_{V=1}}{\Delta^{(IMSA-CG)}\big\rfloor_{V=1}} \simeq 2.80$ and $\frac{\Delta^{(CG)}\big\rfloor_{V=16}}{\Delta^{(IMSA-CG)}\big\rfloor_{V=16}} \simeq 1.90$).

Finally, Fig. 8 shows the images of the reconstructed profiles when the CG-Approach [Figs. 8(a), 8(c), 8(e), 8(g)] and the IMSA-CG Approach [Figs. 8(b), 8(d), 8(f), 8(h)] are used for $V = 1$ [Figs. 8(a), 8(b)], $V = 6$ [Figs. 8(c), 8(d)], $V = 12$ [Figs. 8(e), 8(f)], and $V = 24$ [Figs. 8(g), 8(h)] views, respectively. The two cylinders have been effectively reconstructed, but the reconstruction accuracy gets better when the number of views grows. Moreover, as indicated by the values of the error figures, the retrieval achieved with IMSA-CG Approach turns out to be more close to the actual one when the multi-view setup is adopted. However, it can be remarked that the centers of each cylinders are slightly shifted whatever $V > 1$. Even though such a shift is within the experimental margin, it should be pointed out that a similar behavior has been obtained in several tests with various methods (see [15] for a detailed review). This could suggest that an incorrect positioning occurred during the data measurement.

4. CONCLUSIONS

In this paper, the effect of a multi-view measurement setup on the reconstruction accuracy of the IMSA has been analyzed. The capabilities of the multi-resolution approach to fully exploit the increment of the information content allowed by the multi-view system have been assessed and compared with those of a standard reference method. As a benchmark, some experimental dataset available at the "Institute Fresnel" — Marseille, have been processed and, notwithstanding the large amount of systematic errors that a real measurement setup introduce, the proposed strategy has shown satisfactory performances. The obtained results indicate that the IMSA benefits by multi-illumination conditions in a real environment, as well, and it is able to usefully exploit the allowed increment of information.

REFERENCES

1. Bolomey, J. Ch., "New concept for microwave sensing," *Adv. Microw. Millim. Wave Detectors*, Vol. 2275, 1994.

2. Louis, K., "Medical imaging: State of the art and future development," *Inverse Problems*, Vol. 8, 709–738, 1992.
3. Hoole, R. H. et al., "Inverse problem methodology and finite elements in the identifications of cracks, sources, materials, and their geometry in inaccessible locations," *IEEE Trans. Magn.*, Vol. 27, 3433–3443, 1991.
4. Daniels, D. J., "Surface penetrating radar," *IEE Electron. Comm. Eng. J.*, Vol. 8, 165–182, 1996.
5. Bucci, O. M. and G. Franceschetti, "On the degrees of freedom of scattered fields," *IEEE Trans. on Ant. and Prop.*, Vol. 37, 918–926, 1989.
6. Caorsi, S., G. L. Gragnani, and M. Pastorino, "A multiview microwave imaging system for two-dimensional penetrable objects," *IEEE Trans. Microwave Theory Tech.*, Vol. 39, No. 5, 845–851, 1991.
7. Bucci, O. M. and T. Isernia, "Electromagnetic inverse scattering: Retrievable information and measurement strategies," *Radio Sci.,* Vol. 32, 2123–2138, 1997.
8. Caorsi, S., G. L. Gragnani, and M. Pastorino, "An approach to microwave imaging using a multiview moment method solution for a two-dimensional infinite cylinder," *IEEE Trans. Microwave Theory Tech.*, Vol. 39, No. 6, 1062–1067, 1991.
9. Caorsi, S., M. Donelli, D. Franceschini, and A. Massa, "An iterative multiresolution approach for microwave imaging applications," *Microwave Opt. Tech. Lett.,* Vol. 32, 352–356, 2002.
10. Caorsi, S., M. Donelli, D. Franceschini, and A. Massa, "A new methodology based on an iterative multi-scaling for microwave imaging," *IEEE Trans. Microwave Theory Tech.*, Vol. 51, 1162–1173, 2003.
11. Colton, D. and R. Krees, *Inverse Acoustics and Electromagnetic Scattering Theory,* Springer-Verlag, Berlin, Germany, 1992.
12. Richmond, J. H., "Scattering by a dielectric cylinder of arbitrary cross section shape," *IEEE Trans. Antennas Propagat.*, Vol. 13, 334–341, 1965.
13. Caorsi, S., M. Donelli, and A. Massa, "Location, detection, and imaging of multiple scatterers by means of the iterative multiscaling method," *IEEE Trans. Microwave Theory Tech.*, Vol. 52, 1217–1228, 2004.
14. Kohn, R. V. and A. McKenney, "Numerical implementation of a variational method for electrical impedance tomography," *Inverse Problems*, Vol. 6, 389–414, 1990.

15. Belkebir, K. and M. Saillard, "Testing inversion algorithms against experimental data," *Inverse Problems*, Special section, Vol. 17, 1565–1702, 2001.
16. Weir, W. B., "Automatic measurement of complex dielectric constant and permeability at microwave frequencies," *Proc. IEEE*, Vol. 62, 33–36, 1974.

Massimo Donelli graduated in Electronic Engineering at University of Genoa in 1998 and received the Ph.D. degree in Space Science and Engineering at the same university in 2003. Dr. Donelli is a senior researcher at the Department of Information and Communication Technology, University of Trento, Italy. His main interests are on electromagnetic inverse scattering, adaptive antennas synthesis, optimization techniques for microwave imaging, wave propagation in superconducting materials and in urban environment.

Davide Franceschini received the "master degree" in Telecommunications Engineering from the University of Trento, Italy, in 2003. He is currently a Ph.D. student of the International Graduate School in Information and Communication Technologies, University of Trento, Italy and a member of the ELEDIA Group. His researches are mainly focused on electromagnetic inverse scattering methodologies in industrial processes, medicine, subsurface sensing and propagation of electromagnetic fields in random media.

Gabriele Franceschini, Ph.D. Student received the "master degree" in Telecomunications Engineering at University of Trento, Italy, in 2004. Actually he is a Ph.D. student of International Graduate School in Information and Communication Technologies, University of Trento, Italy. Moreover, he is a member of the ELEDIALab Staff at the same University. His researches are mainly focused on antennas synthesis and design, electromagnetic compatibility and electromagnetic inverse scattering methodologies.

Andrea Massa received the laurea degree in Electronic Engineering from the University of Genoa, Genoa, Italy, in 1992 and Ph.D. degree in Electronics and Computer Science from the same university in 1996. From 1997 to 1999 he was an Assistant Professor of Electromagnetic Fields at the Department of Biophysical and Electronic Engineering (University of Genoa). Since 2000, he has been an Associate Professor at the University of Trento. At present, Prof. Massa is the director of the ELEDIALab at the University of Trento. He is a member of

the PIERS Technical Committee and of the Inter-University Research Center for Interactions Between Electromagnetic Fields and Biological Systems (ICEmB). His research work since 1992 has been principally on electromagnetic direct and inverse scattering, microwave imaging, optimization techniques, wave propagation in presence of nonlinear media, wireless communication and applications of electromagnetic fields to telecommunications, medicine and biology.